Research on Chemical Intermediates (2024) 50:4351–4365
https://doi.org/10.1007/s11164-024-05346-x

Facile synthesis of novel bi-heteroatom functionalized hyper-crosslinked porous polymers with efficient adsorption of methylene blue and methyl orange

Xiaolei Fu[1] · Yan He[1] · Zhulei Guo[1] · Mingfan Chen[1] · Wenlong Du[1] · Yuqin Zeng[1] · Dingzhong Yuan[1] · Bing Na[1]

Received: 1 May 2024 / Accepted: 2 July 2024 / Published online: 17 July 2024

Abstract

In this work, we designed and synthesized two novel bi-heteroatom functionalized hyper-crosslinked porous polymers (HCP-CT and HCP-CF) through a simple one-step Friedel–Crafts alkylation reaction. The resulted polymers N/S bi-heteroatom functionalized polymer HCP-CT and N/O bi-heteroatom functionalized polymer HCP-CF both have good adsorption property for organic dyes such as methyl orange (MO) and methylene blue (MB) in aqueous solution due to its rich pore structure, high specific surface area and rich-heteroatoms of pore surface. It is worth mentioned that the maximum adsorption capacity (q_{max}) of cationic dye MB by the porous polymer HCP-CT at room temperature was reached up to 1571.46 mg/g, which is much higher than that of most reported porous materials. Furthermore, the adsorption capacity of HCP-CT for the cationic dye MB was more than seven times that of the anionic dye MO (q_{max} = 212.77 mg/g). Also, the polymer HCP-CF for the MB adsorption capacity (q_{max} = 352.11 mg/g) was more than twice higher than that of anionic dye MO (q_{max} = 131.75 mg/g). The above trends may be because of the stronger electrostatic interaction between the negatively charged N-S/O bi-heteroatom of HCP-CT and HCP-CF with the cationic dye MB than that of MO. In addition, the removal percentage of polymers HCP-CT and HCP-CF still remained above 80% after five adsorption–desorption cycles. Hence, this work may provide a convenient synthetic route to develop a novel hyper-crosslinked polymer with high capacity for the entrapment of dyes from aqueous solution.

Keywords Hyper-crosslinked porous polymer · Bi-heteroatom · Dyes · Adsorption

Extended author information available on the last page of the article

Introduction

With the development of manufacturing industry, water pollution is becoming more and more serious, and dyes are the most common pollutants in wastewater [1–3]. So, it must be effectively treated the dyes wastewater before discharge, otherwise it will cause great harm to the environment and human health. The common treatment techniques include electrochemical oxidation [4], membrane separation [5], ion exchange [6], photodegradation [7] and adsorption [8–10]. Adsorption is a promising dye removal method among these various dye wastewater treatment methods owing to its simple operation process, low cost and effective [11–14]. The key to adsorption is the adsorbent. Generally, the traditional porous adsorbents are bentonite [15], zeolite [16], clay [17], biochar [18] and activated carbon [19]. However, the above porous adsorbents have some drawbacks such as complicated synthesis process, low dyes adsorption capacity and poor selectivity [8, 20]. Therefore, it is necessary to develop new types of adsorbents with high adsorption capacity for dyes in industrial wastewater.

Very recently, as an emerging solid adsorbent, the hyper-crosslinked porous polymers (HCPs) have attracted much attention due to their diverse synthesis methods, simple functionalization and excellent adsorption capacity [8, 21–24]. Generally, the removal efficiency and selectivity for dyes mainly depend on the functional groups of the adsorbents [25]. Through introduction of characteristic groups such as amino [26], carboxyl [27] and heteroatoms [28] to the HCPs, it thus can facilitate the binding between adsorbents and dyes. For example, Yali Luo [29] prepared carbonaceous materials doped with boron, nitrogen, oxygen, fluorine and sulfur heteroatoms by simple heat treatment using ionic liquids (TSIL) as precursors, and the introduction of multi-heteroatoms enabled the carbonaceous materials to have more efficient adsorption properties for dyes. Nisar Ahamed Babujohn [10] constructed two triphenylene-based crown ether COPs (COP-TPC6 and COP-TPC8). The obtained COP-TPCs displayed good removal capacity toward a wide range of organic dyes like thiazine dye, triarylmethane dye and azo dye via supramolecular non-covalent interaction. COP-TPC6 displayed good removal capacity toward neutral red (NR) ($q_{max} = 500$ mg/g), malachite green (MG) ($q_{max} = 364$ mg/g) and mordant orange (MoO) ($q_{max} = 193.8$ mg/g). He Li[30] prepared a series of nitrogen-doped mesoporous carbon (NMC) materials with different nitrogen contents (9.1–11.3 wt %) by sol–gel method using urea as a nitrogen source, and the materials had good adsorption capacity for methyl orange. However, the adsorption capacity of single heteroatom adsorbent is slow, which seriously limited the application of heteroatom adsorbent in the field of dyes adsorption. Meanwhile, as far as we know, the bi-heteroatom functionalized hyper-crosslinked porous polymers (HCP-CT and HCP-CF) for the dye's adsorption have not been reported.

Herein, we selected the carbazole, thiophene and furan as the N, S, O heteroatom monomer, respectively. Two novel N/S bi-heteroatom functionalized polymer HCP-CT and N/O bi-heteroatom functionalized polymer HCP-CF were obtained by the simple one-step Friedel–Crafts alkylation reaction. The

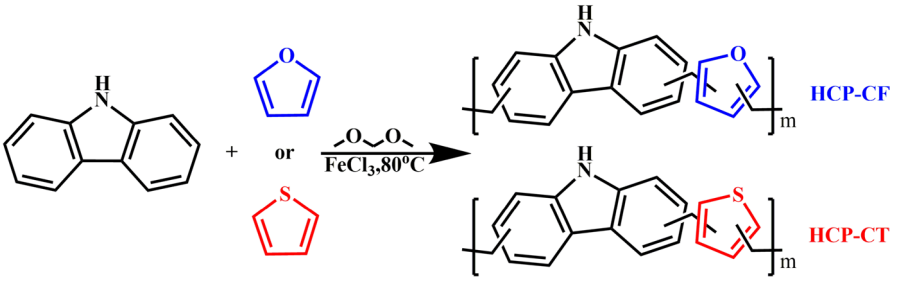

Scheme 1 The synthesis route of bi-heteroatom functionalized polymer HCP-CT and HCP-CF

adsorption kinetics, adsorption isotherms and adsorption cycles of the above bi-heteroatom functionalized hyper-crosslinked porous polymers were performed in detailed. The results show that the bi-heteroatom functionalized materials are efficient adsorbents for adsorption of dyes such as MB and MO.

Experiment

Reagents and materials

The purity of all the reagents used was AR. Methyl orange (MO,96%), methylene blue (MB,90%), Rhodamine B (RB,95%), Reactive blue R(KN-R,99%), carbazole (96%), thiophene (99%), furan (99%), formaldehyde dimethyl acetal (FDA) (98%), anhydrous methanol (99.5%), 1,2-dichloroethane (99%) and anhydrous ferric chloride (98%) were purchased from Aladdin Reagent Co, Ltd.

Synthesis of bi-heteroatom functionalized polymer HCP-CT and HCP-CF

As shown in Scheme 1, the carbazole (5 mmol, 0.8361 g), thiophene (5 mmol, 0.4207 g) or furan (5 mmol, 0.3404 g) were dissolved into a double-necked flask containing 40 ml 1, 2-dichloroethane (DCE). Then the FDA (20 mmol) and anhydrous ferric chloride (10 mmol, 1.62 g) were added to the above solution under nitrogen. The mixtures were heated to 80 ℃ and stirred for 24 h. After the reaction was complete, the product was collected and washed repeatedly with methanol until the filtrate was clarified. The above products were then dried in vacuum for 12 h to obtain N/S bi-heteroatom functionalized polymer HCP-CT and N/O bi-heteroatom functionalized polymer HCP-CF.

Instruments and characterization

The morphology of the samples was observed by field emission scanning electron microscope (SEM, Nova NanoSEM450). Transmission images of the materials were recorded using a transmission electron microscope (JEOLJEM-2100). The crystal property of the sample was analyzed using a polycrystalline X-ray diffractometer

(Germany/D8 ADVANCEA25). N_2 adsorption desorption isotherms at 77 K were measured using a volumetric adsorption analyzer Micromeritics ASAP 2460, USA. The samples were degassed at 120 °C for 24 h. The specific surface area was calculated using the Brunner–Emmett–Taylor (BET) method. The structure of the materials was performed by solid-state ^{13}C NMR (German Bruker Avance Neo 400WB) and the infrared spectra (Nicolet 5700, USA). Thermogravimetric parameters obtained by Netzsch TG 209 F3 Tarsus, Germany. The U(VI) concentration in the medium was determined using a double beam UV/Vis spectrophotometer (UV-XU-6, China).

Adsorption experiment

The pH influence of MB and MO adsorption by HCP-CT and HCP-CF

In this work, the adsorption of HCP-CT and HCP-CF on dyes (such as MB and MO) solutions at different pH values was investigated. We weighed 5 mg of adsorbent powder and added it to 10 ml reaction bottles containing the initial concentrations of 100 mg/L MB and 50 mg/L MO. The pH of the dye solutions was adjusted by adding 0.1 mg/L HCl or 0.1 mg/L NaOH. The pH value of MB solution is 2–12, and the pH value of MO solution is 2–10. Three parallel experiments were set up for all the adsorption experiments.

Study on MB and MO adsorption isotherms of HCP-CT and HCP-CF

The adsorption properties of the HCP-CT and HCP-CF were investigated for different concentrations of MB and MO. Weighed 5 mg adsorbent and added into 10 ml reaction bottles containing different concentrations of dyes. The concentration gradient of MB dye solution was set from 20 to 1000 mg/L. The concentration gradient of MO dye solution was set from 20 to 500 mg/L. After adsorption, the adsorbent and the MO and MB solutions were separated by centrifugation, and the supernatant was taken to measure the concentration of the adsorbed solution with a UV–Vis spectrophotometer and calculate the removal percentage. The adsorption capacity of dyes on HCP-CT and HCP-CF and the removal percentage were calculated according to the following equations.

$$q_c = \frac{\left(C_0 - C_e\right) \times V}{m} \tag{1}$$

$$\mathrm{R\%} = \frac{\left(\mathrm{C_0} - \mathrm{C}_e\right)}{\mathrm{C_0}} \times 100\% \tag{2}$$

where q_e represents the adsorption capacity (mg/g) when the adsorption reaches equilibrium. C_0 is the initial concentration (mg/L) of MB or MO solution before adsorption. C_e represents the equilibrium concentration (mg/L) of MB and MO

solution after adsorption. *R*% is the removal percentage of dye MB and MO in the solution.

Study on MB and MO adsorption kinetics of HCP-CT and HCP-CF

The effect of different adsorption times on the adsorption of methylene blue (MB) and methyl orange (MO) by HCP-CT and HCP-CF was investigated. 5 mg of adsorbent powder was added to a 10 ml reaction bottles containing a solution of 10 mL of 100 mg/L MB and 10 mL of 100 mg/L MO dye, respectively. The adsorption time in the mechanical shaker was tested for 0 min-300 min, respectively. Three parallel experiments were set up for all the adsorption experiments.

Study on the reusability of HCP-CT and HCP-CF

In order to investigate the reusability of the HCP-CT and HCP-CF, five desorption–adsorption cycles of HCP-CT and HCP-CF were tested with ethanol. 25 mg of HCP-CT and HCP-CF, the cationic dye MB ($C_0 = 100$ mg/L, pH = 8, $t = 150$ min) and the anionic dye MO ($C_0 = 50$ mg/L, pH = 6, $t = 120$ min) were added to a 50 mL reaction bottles. After adsorption, the dye containing the HCP-CT and HCP-CF adsorbents was washed with deionized water. The polymers were then desorbed with anhydrous ethanol. After vacuum drying at 80 °C, the next round of adsorption–desorption was carried out, and the above experiment was repeated five times.

The selectivity of HCP-CT and HCP-CF

Different concentrations with 40 mg/L, 60 mg/L, 80 mg/L and 100 mg/L dyes mixed solutions were prepared. Then 5 mg of HCP-CT and HCP-CF adsorbents was placed in 20 mL of the above mixed dye solutions with different gradients. The adsorption time in the mechanical shaker was set 180 min, and the dye selectivity performance was tested. The absorbance values of different dyes at the corresponding absorption wavelengths ($\lambda_{MO} = 465$ nm; $\lambda_{KN\text{-}R} = 591$ nm; $\lambda_{MB} = 664$ nm; $\lambda_{RB} = 554$ nm) were measured using a UV/Vis spectrophotometer.

Results and discussion

Characterization

In order to characterize the chemical structure of HCP-CT and HCP-CF, the infrared spectroscopy was performed. As shown in Fig. 1a, the main absorption peaks at 600–1500 cm^{-1} come from the stretching and bending vibrations of the carbazole ring [31]. The vibration peak at 743 cm^{-1} is attributed to the C–S [32], indicating the thiophene successfully cross-linked with carbazole into the porous polymer HCP-CT. Likewise, the vibration peak at 1150 cm^{-1} is attributed to the C–O–C [33], indicating the vibration peak of the furan ring in HCP-CF. Furthermore, its structure was also confirmed by (CP/MAS) ^{13}C NMR (Fig. 1b). The

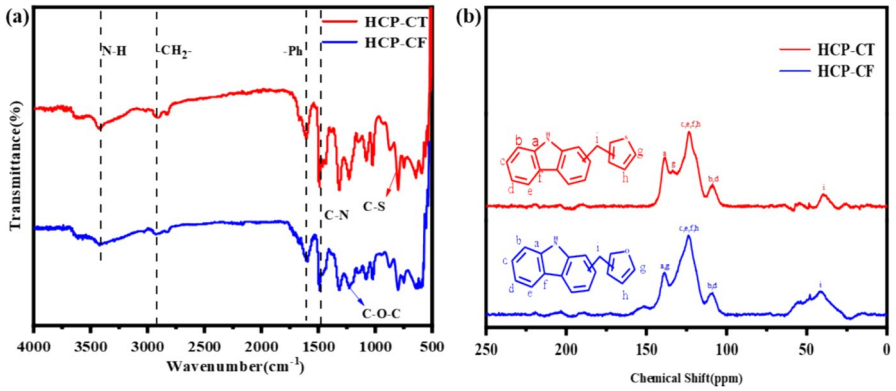

Fig. 1 **a** FTIR spectra of HCP-CT and HCP-CF, **b** the ^{13}C NMR patterns of HCP-CT and HCP-CF

resonance peak at 148.6 ppm originates from the aromatic carbon of the carbazole ring. The two carbon peaks in the aromatic ring are located at 123.7 and 110.6 ppm, respectively. Most importantly, the peak at 37.5 ppm is clearly indicative of the methylene carbon that is formed by the Friedel–Crafts alkylation reaction [21, 34–36]. Therefore, carbazole monomers have successfully been cross-linked with and thiophene or furan monomers by the methylene bond into the copolymers HCP-CT and HCP-CF.

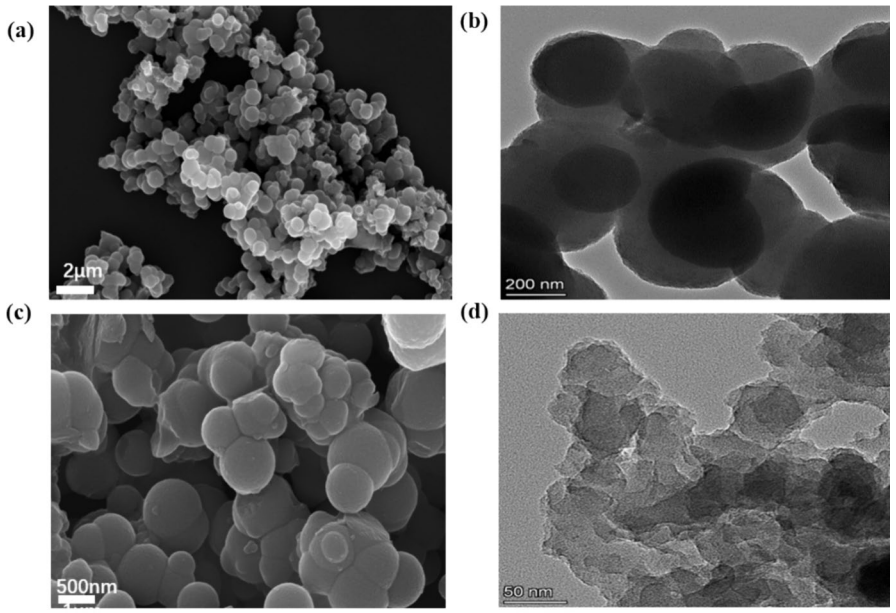

Fig. 2 **a** The SEM image of HCP-CT, **b** the TEM image of HCP-CT, **c** the SEM image of HCP-CF, **d** the TEM image of HCP-CF

The morphology of HCP-CT and HCP-CF was characterized by SEM and TEM. Figure 2a, c shows that the morphologies of HCP-CT and HCP-CF both form a relatively regular cluster-like spherical structure with submicron particles. Moreover, the TEM images (Fig. 2b, d) completely consistent with the SEM characterization structure. And all samples possess amorphous microporosity (Fig. S1 and S2, Supporting Information). In addition, without any characteristic peaks in all XRD patterns (Fig. 3a), it confirms the amorphous nature of all polymers.

As shown in Fig. 3b, thermogravimetric analysis (TGA) results show that the properties of HCP-CT and HCP-CF are relatively stable. The first loss of bi-heteroatom functionalized polymer HCP-CT and HCP-CF at 80–100 °C may be caused by the release of entrapped solvent or some small gaseous molecules (such as methanol and dichloroethane). The second weight loss occurred between 100 and 400 °C, which may be caused by the gradual decrease of guest molecules. The mass of materials HCP-CT and HCP-CF can be still maintained more than 50% at 800 °C, indicating that the two materials have good thermal stability. It is worth mentioned that high thermal stability of these hyper-crosslinked porous polymer HCP-CT and HCP-CF is good enough for their potential applications in water treatment.

The porosity of the N/S bi-heteroatom functionalized polymer HCP-CT and N/O bi-heteroatom functionalized polymer HCP-CF is determined by the N_2 adsorption–desorption isotherm at 77K. As shown in Fig. 4a, adsorption initially increases sharply at low pressures ($p/p_0 < 0.1$) with obvious microporosity. At relative pressures above 0.9, hysteresis loops indicate the presence of macroporous and interporous voids. There is hysteresis in the N_2 desorption curves of these polymers, which is usually attributed to the swelling effect of the polymer network in contact with nitrogen. In addition, the pore size distribution (PSD) curves calculated according to the non-local density theory (NDFT) are shown in Fig. 4b, which further confirms that micropores (~2 nm) are predominantly presented in HCP-CT and HCP-CF. The BET-specific surface areas of HCP-CT and HCP-CF are 622.07 m^2/g and 466.44 m^2/g, respectively. The porosity parameters are given in Table 1. The bi-heteroatom functionalized hyper-crosslinked porous polymer HCP-CT and HCP-CF

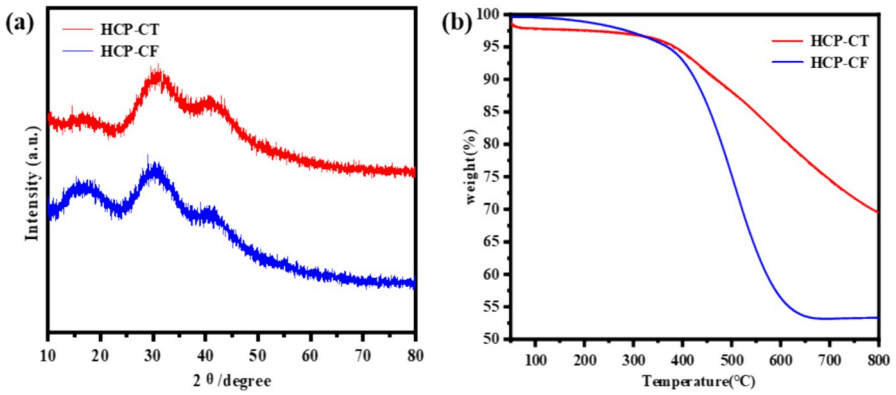

Fig. 3 **a** XRD of HCP-CT and HCP-CF, **b** the TG patterns of HCP-CT and HCP-CF

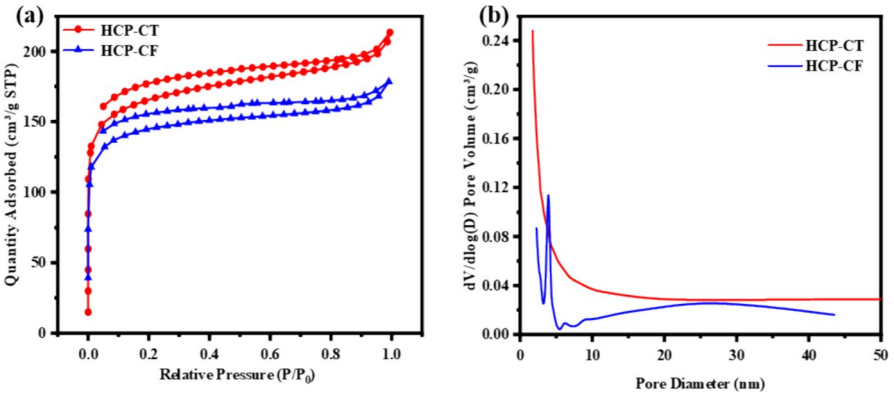

Fig. 4 **a** N_2 adsorption–desorption isotherms of HCP-CT and HCP-CF, **b** the pore size distribution of HCP-CT and HCP-CF

Table 1 Specific surface area and pore volume of HCP-CT and HCP-CF

Materials	BET surface area (m^2/g)	Pore volume (m^3/g)
HCP-CT	622.07	0.33
HCP-CF	466.44	0.28

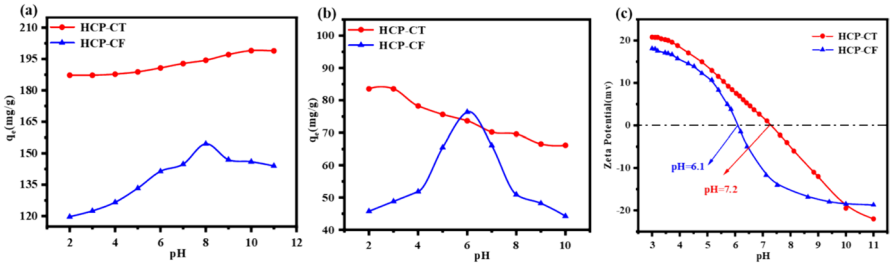

Fig. 5 The influence of pH on the adsorption effect of MB (C_0 = 100 mg/L, T = 25 °C, m/v = 0.5 g/L) (**a**) and MO (C_0 = 50 mg/L, T = 25 °C, m/v = 0.5 g/L), **c** Zeta potential of HCP-CT and HCP-CF

have a large specific surface area, which is conducive to the enhancement of the adsorption capacity of dyes.

Dyes adsorption

pH effect on the adsorption of MB and MO

The pH of the solution plays a key role in the adsorption of dyes by polymers. Figure 5c shows that the zero potential points (pHzpv) of HCP-CT and HCP-CF are

pH = 7.2 and pH = 6.1, respectively. When the pH value is low (pH < pHzpv), the surface of the two polymers will be protonated and thus gain positive charge, which is beneficial to the adsorption of anionic dyes by the polymers. As shown in Fig. 5a, the adsorption capacity of MB increased with the increase of pH (pH < 8), which is attributed to the increase of deprotonation of the functional groups on the surface of HCP-CF. At pH 8–10, the adsorption capacity of MB decreased with increasing pH and reached the maximum at pH 8. At pH 8, HCP-CF was able to obtain a negative surface charge, which was reacting a strong electrostatic attraction between the negative surface charge of HCP-CF and the MB cation. HCP-CT had a higher negative potential under the strong alkaline condition and the adsorption capacity of HCP-CT on MB reached the maximum value at pH 10. Therefore, in the following experiments, HCP-CF adsorbed MB using pH = 8, and HCP-CT adsorbed MB using pH = 10.

However, for the MO adsorption, the pH effect trends are different from the MB adsorption. When the pH is low (pH < pHzpv), HCP-CT shows good adsorption capacity on MO. In the presence of strong acids, a large amount of H^+ will have a strong electrostatic repulsion, which prevented the dye molecules from contacting with HCP-CT and HCP-CF. When the pH is greater than 3, with the increase of pH, the adsorption capacity of HCP-CT on MO becomes decrease. Meanwhile, the adsorption effect of HCP-CF on MO is stronger, reaching the highest adsorption capacity at pH = 6. Therefore, in the following experiments, HCP-CF adsorbed MO using pH = 3, and HCP-CT adsorbed MO using pH = 6.

Adsorption kinetics of MB and MO

The adsorption kinetics MO and MB by HCP-CT and HCP-CF within 0–300 min was studied. Figure 6a, c shows that the adsorption of organic dyes (MB and MO) by HCP-CT and HCP-CF increased rapidly within the first 15 min, which was attributed to the large number of reactive heteroatom sites on the surface of HCP-CT and HCP-CF. As the contact time increases, the heteroatom sites become saturated and the adsorption capacity reaches equilibrium. When HCP-CT and HCP-CF adsorbed MO, the adsorption equilibrium time was 60 min and 90 min, respectively. The adsorption equilibrium time of HCP-CT and HCP-CF on MB was 60 min and 150 min, respectively. Because the S atoms of the HCP-CT possess lone pair electrons, which provide active sites through dipole–dipole interaction. While the O atom of HCP-CF also has lone pair electrons, its de-electronic ability is less than S atoms. So, when the HCP-CF adsorption of organic dyes (MB and MO), the structure's changes resulted in a longer adsorption time. In the subsequent experiments, the contact time between the adsorbent material and the dye solution was set at 180 min in order to achieve complete adsorption of the dye by the material.

In order to study the adsorption kinetic properties of HCP-CT and HCP-CF, the adsorption data of MO and MB were fitted with three kinetic models. As shown in Fig. S3 (Supporting Information), the point distribution fitted by the pseudo-first-order kinetic model of HCP-CT and HCP-CF is uneven. As listed in Tables S1 and S2 (Supporting Information), the linear coefficient R^2 of pseudo-first-order kinetics is smaller than that of pseudo-second-order kinetic model. Therefore, the adsorption

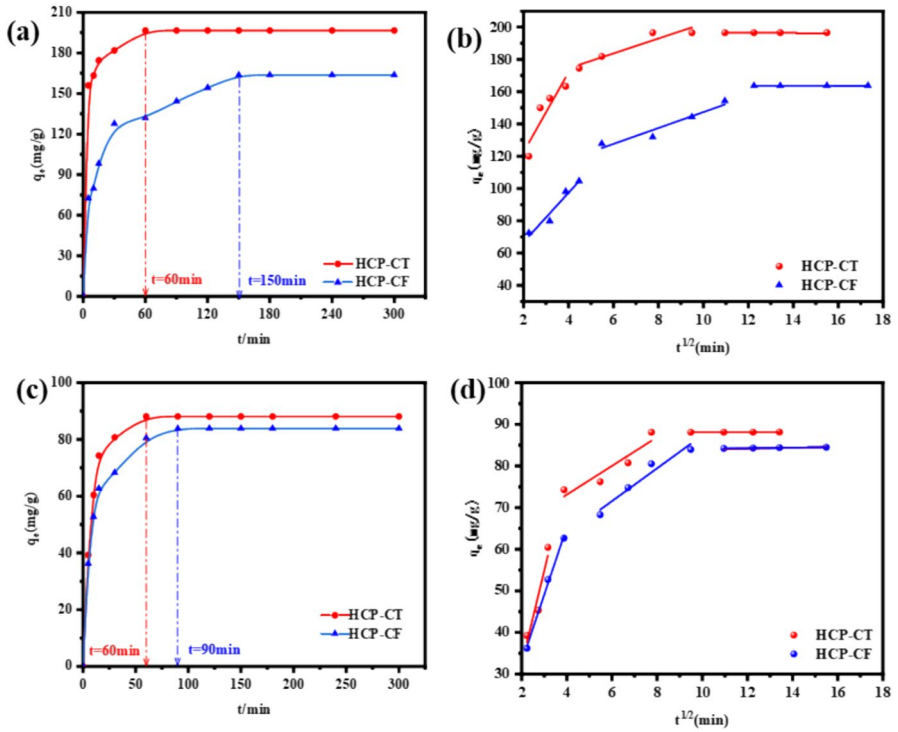

Fig. 6 **a** Adsorption kinetic curve of HCP-CT and HCP-CF in MB (C_0 = 100 mg/L, T = 25 °C, m/v = 0.5 g/L) and **c** MO (C_0 = 50 mg/L, T = 25 °C, m/v = 0.5 g/L), intraparticle diffusion fitting curves of adsorption **b** MB and **d** MO

process of organic dyes (MO and MB) by HCP-CT and HCP-CF was more fitted with the pseudo-second-order kinetic model, indicating that the adsorption process of HCP-CT and HCP-CF had both physical adsorption and chemical adsorption, and is greatly affected by chemical adsorption. In addition, the intraparticle diffusion model (Fig. 6b, d) was fitted to the adsorption kinetics of the material. It can be seen that the adsorption process of the material was divided into three stages, namely, surface adsorption, intraparticle diffusion and equilibrium adsorption of the material. As shown in Tables S3 and S4 (Supporting Information), the adsorption process of the material is dominated by the surface adsorption of the material and the trend of surface adsorption of the material is more obvious in MO.

Adsorption isotherms of MB and MO

In order to study the adsorption behavior of bi-heteroatom functionalized polymer HCP-CT and HCP-CF, the adsorption isotherms can well describe the adsorption process of HCP-CT and HCP-CF. At different initial concentrations, the adsorption isotherms of HCP-CT and HCP-CF on organic dyes MO and MB are shown

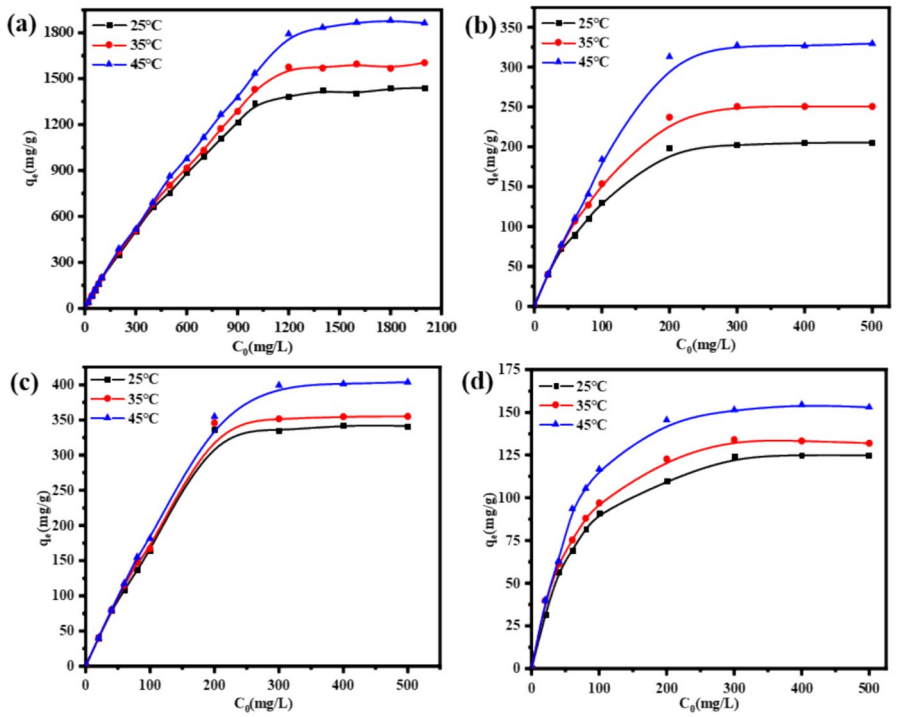

Fig. 7 The adsorption isotherms of **a** HCP-CT of MB, **b** HCP-CT of MO, **c** HCP-CF of MB, **d** HCP-CF of MO (MB: pH = 8, t = 150min, m/v = 0.5 g/L; MO: pH = 6, t = 120min, m/v = 0.5 g/L)

in Fig. 7. When the initial concentration of the dye solution is low, the adsorption capacity of HCP-CT and HCP-CF increases with the increase of the concentration. This is because HCP-CT and HCP-CF can provide sufficient adsorption sites for dye molecules, so the adsorption rate is fast and the adsorption capacity increases rapidly. As the initial concentration of MO and MB increased, the dyes adsorption capacity increased due to more adsorption sites on the adsorbent surface bound the dye molecules. The adsorption capacity reached equilibrium when the initial concentration of MO or MB reached a certain level.

The adsorption behavior of HCP-CT and HCP-CF was further discussed using Langmuir and Freundlich models. As shown in Fig. S4 (Supporting Information), the fitting correlation coefficient R^2 of the Langmuir isotherm model is larger than that of the Freundlich isotherm model. So, the adsorption process of the dyes MB and MO by HCP-CT and HCP-CF is more consistent with the Langmuir monolayer adsorption model. The MO maximum adsorption capacity of HCP-CT and HCP-CF calculated by Langmuir model was 212.77 mg/g and 131.75 mg/g, respectively. The MB maximum adsorption capacity of HCP-CT and HCP-CF calculated by Langmuir model was 1571.46 mg/g and 352.11 mg/g, respectively. The above trends may be because of the stronger electrostatic interaction between the negatively charged N-S/O bi-heteroatom of HCP-CT and HCP-CF with the cationic dye MB than that of MO. As listed Table 2, the MB and MO adsorption capacity by the bi-heteroatom

Table 2 Comparison of MO and MB adsorption capacities with recent porous polymeric materials and the materials in this work

Adsorbents	BET(m^2/g)	q_{max} of MB	q_{max} of MO	References
UiO-66-NH_2	953.7	549.6	148.4	[37]
GCA	62.06	110.9	543.4	[38]
UIO-g-NL	511.05	1120.7	961.54	[39]
UPCH800	1206.95	227.53	417.34	[40]
ZIF-67	304.5	185.67	130.2	[41]
CSAC	542.06	217.35	73.3	[42]
CHS-CSAC	498.67	209.4	105.2	[42]
HCP-CT	622.07	1571.46	212.77	This work
HCP-CF	466.44	352.11	131.75	This work

functionalized hyper-crosslinked porous polymer HCP-CT and HCP-CF is much higher than that of some reported porous polymer [37–42]. Moreover, the adsorption capacity of HCP-CT and HCP-CF to MO and MB at different temperatures was studied. The results showed that the dyes maximum adsorption capacity increased as the temperature increased, suggesting the adsorption of MO and MB on HCP-CT and HCP-CF is favorable at high temperature conditions. In addition, the other cationic dye RB and anionic dye KN-R were also adsorbed by the HCP-CT and HCP-CF. As shown in Fig. S5 (Supporting Information), at different concentrations, the cationic dye (MB and RB) adsorption capacity was higher than the anionic dye (MO and KN-R).

Desorption and regeneration

The pH study and adsorption isotherms show that HCP-CT and HCP-CF are a class of highly efficient MB and MO adsorbents because of their large porosity, large surface area and double heteroatom synergistic effect. Therefore, in the study of the desorption process of HCP-CT and HCP-CF on dyes, it was found that MB and MO

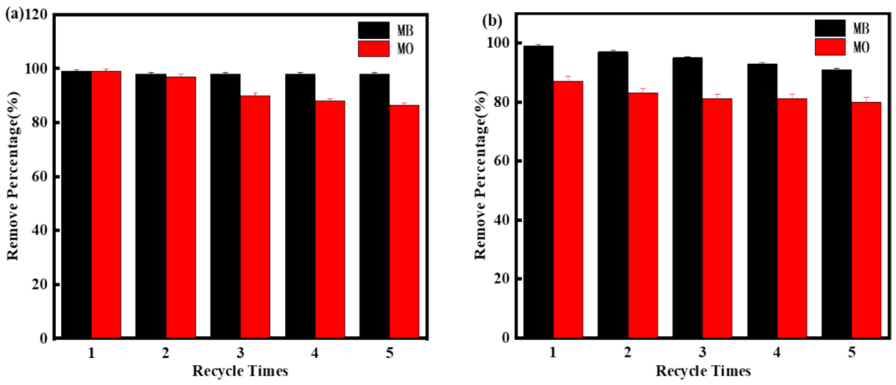

Fig. 8 **a** The recycle times of HCP-CT, **b** the recycle times of HCP-CF

could be desorbed from HCP-CT and HCP-CF by hydrochloric acid washing. The desorption efficiency can reach 80%. In order to prove the reusability of HCP-CT and HCP-CF, we repeated five adsorption–desorption cycles. As shown in Fig. 8, the removal percentage of HCP-CT and HCP-CF did not change significantly during the adsorption–desorption cycle. The results show that HCP-CT and HCP-CF adsorbents are suitable for the efficient removal of dyes in aqueous solution.

Conclusion

Through a simple one-step Friedel–Crafts alkylation strategy, two novel bi-heteroatom functionalized hyper-crosslinked porous polymers (HCP-CT and HCP-CF) were obtained. The BET-specific surface areas of the obtained polymers N/S bi-heteroatom functionalized polymer HCP-CT and N/O bi-heteroatom functionalized polymer HCP-CF are 622.07 m^2/g and 466.44 m^2/g, respectively. And HCP-CT and HCP-CF have high adsorption efficiencies for MB and MO in aqueous solution. The adsorption behavior of MB and MO by HCP-CT and HCP-CF fitted to pseudo-second-order kinetics and Langmuir monolayer adsorption model. The maximum adsorption capacity of MB and MO by HCP-CT at room temperature calculated by Langmuir model was 1571.46 mg/g and 212.77 mg/g, respectively. Furthermore, the used HCP-CT and HCP-CF can be effectively reused at least five times without significant loss of adsorption capacity. Therefore, HCP-CT and HCP-CF have broad applications in water purification and treatment fields.

Supplementary Information The online version contains supplementary material available at https://doi.org/10.1007/s11164-024-05346-x.

Acknowledgements Financial support for this work was provided by the National Science Foundation of China (21908022,22066002), the Jiangxi Provincial Natural Science Foundation (20202BAB213009), Jiangxi Provincial Key Innovation Project (202110405013), Experimental Technology Development Project of East China University of Technology (1310610123) and the Scientific and Technical Project of the Educational Department in Jiangxi Province (GJJ18040303).

Author contributions Yan He was involved in conceptualization, methodology, investigation, writing—review and editing and project administration. Xiaolei Fu contributed to investigation, formal analysis, writing—original draft preparation and material preparation. Zhulei Guo participated in investigation, formal analysis and material preparation. Mingfan Chen took part in software, formal analysis and writing—original draft. Wenlong Du was responsible for material preparation and date curation. Yuqin Zeng took part in investigation and material preparation. Dingzhong Yuan was involved in writing—review and editing. Bing Na was responsible for resources and writing—review and editing.

Declarations

Conflict of interest The authors declare no competing financial interest and ethical.

References

1. D. Lan, H. Zhu, J. Zhang, S. Li, Q. Chen, C. Wang, T. Wu, M. Xu, Chemosphere **19**, 293 (2022)
2. M. Kanani, V. Javanbakht, Res. Chem. Intermed. **49**, 717 (2023)

3. S. Talaiekhozani, J. Rezania, Water Process. Eng. **19**, 321 (2017)
4. A.B. Isaev, N.S. Shabanov, A.G. Magomedova, P.V. Nidheesh, M.A. Oturan, Environ. Chem. Lett. **21**, 5 (2023)
5. H. Chen, Y.J. Zhang, P.Y. He, C.J. Li, H. Li, Appl. Surf. Sci. **515**, 146024 (2020)
6. J. Joseph, R.C. Radhakrishnan, J.K. Johnson, S.P. Joy, J. Thomas, Mater. Chem. Phys. **242**, 122488 (2020)
7. M.G. Kotp, C.L. Chang, A.F. EL-Mahdy, J. Water Process. Eng. **53**, 103675 (2023)
8. F.N.U. Huhe, J. King, S.S.C. Chuang, Res. Chem. Intermed. **49**, 791 (2023)
9. M.G. Kotp, S.U. Sharma, J.-T. Lee, F.M. EL-Mahdy, J. Taiwan Inst. Chem. E. **134**, 104310 (2022)
10. N.A. Babujohn, A. Eluri, V.P. Nabeela, Chem. Eng. J. **464**, 142459 (2023)
11. N.A. Babujohn, P.A. Shifana, A. Eluri, K.S. Thahaliya, Sep. Purif. Technol. **316**, 123770 (2023)
12. A. Eluri, K. Sairam, J.D. Halpara, N.A. Babujohn, ACS Appl. Polym. Mater. **4**, 10 (2022)
13. C. Jiang, X. Wang, D. Qin, W. Da, B. Hou, C. Hao, J. Wu, J. Hazard. Mater. **369**, 50 (2019)
14. P. Huang, A. Kazlauciunas, R. Menzel, L. Lin, A.C.S. Appl, Mater. Interfaces **9**, 31 (2017)
15. Z. Huang, Y. Li, W. Chen, J. Shi, N. Zhang, X. Wang, Z. Li, L. Gao, Y. Zhang, Mater. Chem. Phys. **202**, 266 (2017)
16. K. Hutsul, I. Ivanenko, L. Patrylak, O. Pertko, D. Kamenskyh, Appl. Nanosci. **13**, 12 (2023)
17. M. Kausar, A. Iqbal, K. Javed, Z.H. Aftab, H. Nazli, H.N. Bhatti, S. Nouren, J. Mol. Liq. **256**, 395 (2018)
18. S. Praveen, J. Jegan, T. Bhagavathi Pushpa, R. Gokulan, L. Bulgariu, Biochar. **4**, 1 (2022)
19. K. Azam, N. Shezad, I. Shafiq, P. Akhter, F. Akhtar, F. Jamil, S. Shafique, Y.-K. Park, M. Hussain, Chemosphere **306**, 135566 (2022)
20. K. Durairaj, P. Senthilkumar, P. Velmurugan, S. Divyabharathi, D. Kavitha, Int. J. Green Energy **16**, 7 (2019)
21. Y. He, Z. Guo, M. Chen, S. Wan, N. Peng, X. Fu, D. Yuan, B. Na, J. Porous Mater. **30**, 5 (2023)
22. L. Feng, S. Lu, H. Zou, G. Chen, D. Xiang, Res. Chem. Intermed. **50**, 2051 (2024)
23. M.G. Kotp, N.L. Torad, H. Nara, W. Chaikittisilp, J. You, Y. Yamauchi, F.M. EL-Mahdy, S.-W. Kuo, J. Mater. Chem. A. **11**(27), 15022 (2023)
24. M.G. Kotp, A.F. EL-Mahdy, T.L. Yang, S.W. Kuo, Micropor. Mesopor. Mater. **331**, 111669 (2022)
25. X.-Q. Wang, M. Zhang, J. Yang, J. Yang, H. Duan, J. Mol. Struct. **1291**, 136018 (2023)
26. M. Van Melkebeke, T. De Somer, T. Van Laere, L.M.T. Nguyen, H.M. Shirazi, H. Poelman, K. Van Geem, S. De Meester, Sep. Purif. Technol. **331**, 125559 (2024)
27. J. Xue, E. Zhu, H. Zhu, D. Liu, H. Cai, C. Xiong, Q. Yang, Z. Shi, Cellulose **30**, 3 (2023)
28. X.-C. Du, J.-H. Zhu, Z.-J. Quan, X.-C. Wang, New J. Chem. **45**, 7 (2021)
29. Y. Luo, Z. Yang, W. Guo, H. Chen, T. Wang, Y. Liu, Y. Lyu, H. Luo, S. Dai, J. Mater. Chem. A **8**(9), 30 (2020)
30. H. Li, N. An, G. Liu, J. Li, N. Liu, M. Jia, W. Zhang, X. Yuan, J. Colloid Interface Sci. **466**, 343 (2016)
31. Q. Meng, Y. Liu, Y. Luo, Y. Lyu, Polym. Bull. **78**, 6 (2021)
32. S. Gupta, A. Mishra, R. Kumar, A. Patra, React. Funct. Polym. **165**, 104972 (2021)
33. I.-V. Ganea, A. Nan, C. Baciu, R. Turcu, Nanomaterials **11**, 3 (2021)
34. Y. Yuan, H. Huang, L. Chen, Y. Chen, Macromolecules **50**, 13 (2017)
35. Q. Zhang, Y. Wang, J. Gong, X. Zhang, Dyes Pigments **184**, 108652 (2021)
36. A. Ilnicka, P. Kamedulski, H.M. Aly, J.P. Lukaszewicz, Arab. J. Chem. **13**, 5 (2020)
37. S.-W. Lv, J.-M. Liu, H. Ma, Micropor. Mesopor. Mater. **282**, 171 (2019)
38. Y. Shi, G. Song, A. Li, Colloid Surfaces A **641**, 128595 (2022)
39. C. Wang, X. Feng, S. Shang, Bioresour. Technol. **388**, 129781 (2023)
40. X. Yuan, X. Wang, S. Hu, Sep. Purif. Technol. **343**, 127169 (2024)
41. T. Qiang, S. Wang, Z. Wang, J. Ind. Eng. Chem. **116**, 371 (2022)
42. A.S. Kamdod, M.V.P. Kumar, J. Poly. Environ. **30**, 12 (2022)

Authors and Affiliations

Xiaolei Fu[1] · Yan He[1] · Zhulei Guo[1] · Mingfan Chen[1] · Wenlong Du[1] · Yuqin Zeng[1] · Dingzhong Yuan[1] · Bing Na[1]

✉ Yan He
yanheecust@163.com

Xiaolei Fu
3508133201@qq.com

Zhulei Guo
928243486@qq.com

Mingfan Chen
2894948186@qq.com

Wenlong Du
2072327989@qq.com

Yuqin Zeng
2625468322@qq.com

Dingzhong Yuan
ydz3214@126.com

Bing Na
bna@ecut.edu.cn

[1] Jiangxi Province Key Laboratory of Functional Organic Polymers, School of Chemistry and Materials Science, East China University of Technology, Nanchang 330013, China